A Role for Advanced Glycation End Products in Diminished Bone Healing in Type 1 Diabetes

Ronaldo B. Santana,[1] Lei Xu,[1] Hermik Babakhanlou Chase,[1] Salomon Amar,[1,2] Dana T. Graves,[1,2] and Philip C. Trackman[1,2]

The effect of type 1 diabetes on bone healing and bone formation in standardized craniotomy defects created in BALB/cByJ mice was determined. The hypothesis that advanced glycation end products (AGEs) contribute to diminished bone healing in diabetes was evaluated by assessing for the presence of the receptor for advanced glycation end products (RAGE) by immunohistochemistry in healing craniotomy defects in diabetic animals. The effect of local application of a known RAGE protein ligand, N^{ϵ}-(carboxymethyl)lysine (CML)−mouse serum albumin (MSA), on craniotomy defect healing in normal animals was then assessed and compared to the effects of control MSA. Finally, evidence in support of the expression of RAGE mRNA and protein in osteoblastic cells was obtained. The results indicated that craniotomy defects in diabetic animals healed ~40% of the degree to which they healed in nondiabetic animals ($P < 0.05$). RAGE was expressed at higher levels in healing bone tissues in diabetic compared to control animals. Further studies in nondiabetic animals indicated that bone healing was reduced by 63 and 42% in lesions treated with 900 and 90 μg CML-MSA, respectively, compared to in animals treated with MSA alone ($P < 0.05$). Evidence for the expression of RAGE was obtained in mouse and rat osteoblastic cultures. These results support the contribution of AGEs to diminished bone healing in type 1 diabetes, possibly mediated by RAGE. *Diabetes* 52:1502–1510, 2003

Alterations in calcium, phosphate, and bone metabolism occur in patients with diabetes (1–4). Reductions in bone mineral content (4,5), osteopenia (6), increased fracture rates (7), and delayed fracture healing (8) characterize diabetic bone disease (9,10). Osteopenia occurs in association with type 1 diabetes, and evidence of reduced osteoblast activity has reported (11–14). The mechanisms that cause diabetic osteopenia have not been clearly identified. Increased nonenzymatic protein glycation occurs in diabetes, leading to the formation of a variety of chemically modified proteins known as advanced glycation end products (AGEs) (15,16). AGEs accumulate in tissues with diabetic complications, including vascular and periodontal tissues, kidney, and bone (17–22). Studies in nonmineralized tissues have shown that AGEs contribute to the pathogenesis of diabetic complications (17). With regard to periodontal tissue, it is now understood that AGEs contribute to increased diabetic alveolar bone loss in periodontal disease in mice (19).

The accumulation of AGE proteins leads to tissue damage through a variety of mechanisms, including structural modification of proteins (23), stimulation of cellular responses via receptors specific for AGE proteins (24,25), and generation of reactive oxygen intermediates (26,27). Among the different known receptors for AGEs, the receptor for AGEs (RAGE) is expressed by a variety of different cell types (28). AGE-RAGE interactions result in the generation of reactive oxygen species and in NF-κB activation in endothelial and smooth muscle cells, which could in turn contribute to the tissue damage and metabolic imbalances seen in diabetic complications (20,29).

Biochemical and immunohistochemical studies indicate that N^{ϵ}-(carboxymethyl)lysine (CML)-modified proteins are AGEs that accumulate in vivo (30–34). CML levels are elevated in the serum of diabetic patients (20,30,34) and bind and activate RAGE signaling (20). The present study was undertaken in part to evaluate the hypothesis that AGE-RAGE interactions contribute to the pathogenesis of diminished bone formation in diabetes.

RESEARCH DESIGN AND METHODS

Diabetes induction and characterization. In vivo experiments were performed in BALB/cByJ mice (Jackson Laboratories, Bar Harbor, ME). Male animals, age 8 weeks, were maintained according to approved protocols (Boston University Institutional Animal Care and Use Committee), and were given free access to tap water and NIH31M mouse diet (5K52; Purina Mills). Generation of diabetic and control nondiabetic animals was accomplished using the multiple low-dosage streptozotocin (STZ) methodology (35). The number of animals per experimental group was six, unless otherwise indicated.

The diabetic condition was characterized. Blood glucose (Accu-Check Advantage; Roche Diagnostics), and urine glucose levels (Multistix 10SG reagent strips; Bayer) were monitored twice weekly throughout the typical 33-day experimental periods, and diabetes onset on experimental day 12 was confirmed in all diabetic animals (blood glucose levels ≥250 mg/dl). Blood and urine glucose values for control animals were normal (100–110 mg/dl). Protein and ketones in the urine were assayed twice weekly and were not detected (Multisix 10SG reagent strips; Bayer). Levels of GHb in blood (Glyc-Affin GHb; Isolab, Akron, OH) and levels of insulin in serum (Linco Research, St. Charles, MO) were measured when animals were killed.

Uniform craniotomy defects. Uniform craniotomy defects were created on day 19, 7 days after confirmation of diabetes onset. General anesthesia of the animals was accomplished by intraperitoneal injection of 0.12 ml/100 g body

From the [1]Boston University Goldman School of Dental Medicine, Division of Oral Biology, Boston, Massachusetts; and [2]Boston University School of Medicine, Biochemistry, Boston, Massachusetts.

Address correspondence and reprint requests to Dr. Philip C. Trackman, Boston University Goldman School of Dental Medicine, Department of Periodontology and Oral Biology, 100 East Newton St., Rm. G-07, Boston, MA 02118. E-mail: trackman@bu.edu.

Received for publication 6 August 2002 and accepted in revised form 18 February 2003.

AGE, advanced glycation end product; CML, N^{ϵ}-(carboxymethyl)lysine; MSA, mouse serum albumin; RAGE, AGE receptor; STZ, streptozotocin.

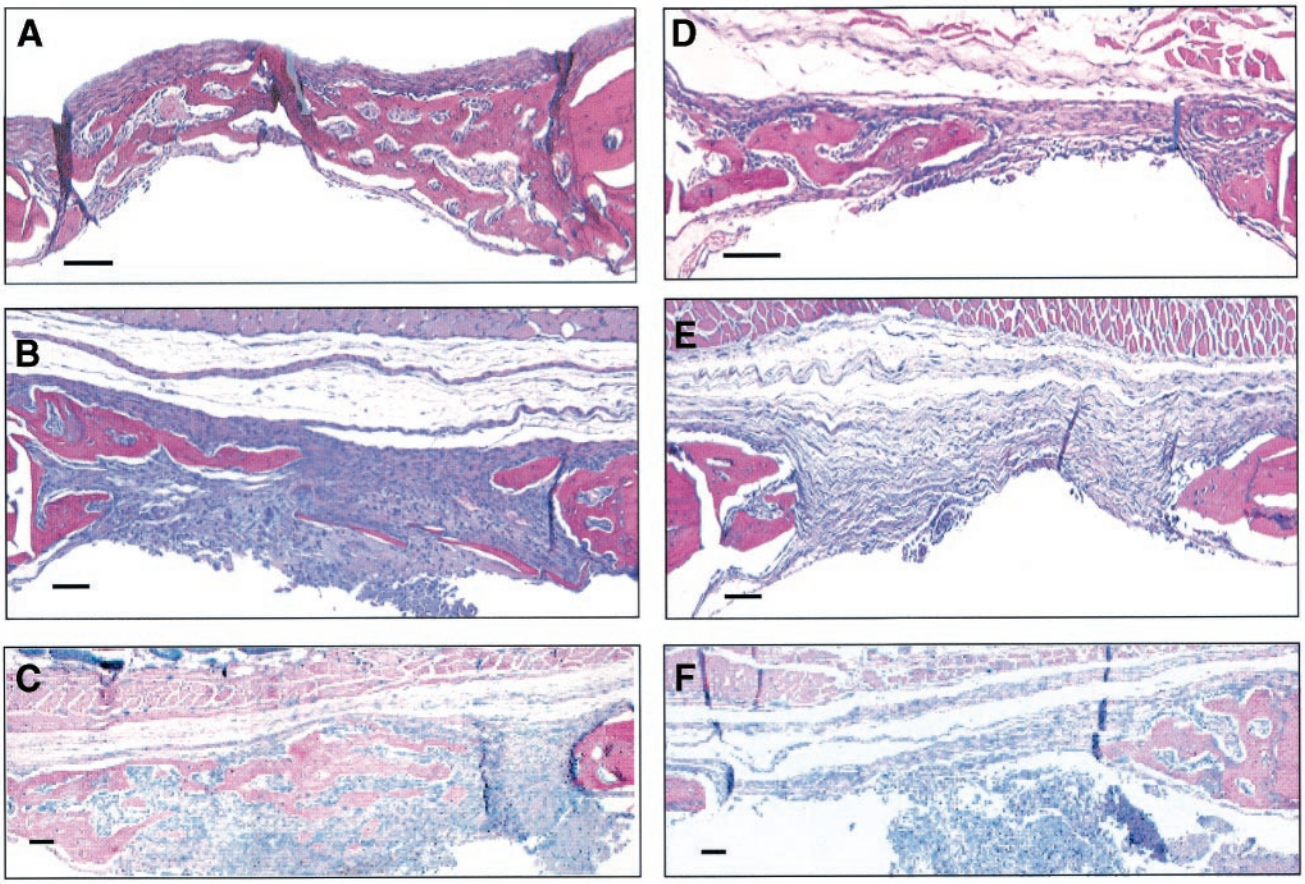

FIG. 1. Histology of standardized bone defects in diabetic and nondiabetic animals harvested after 2 weeks of healing. Slides are from representative specimens stained with hematoxylin and eosin. *A*: Nondiabetic animal, 1.0-mm bone defect; *B*: nondiabetic animal, 1.6-mm bone defect; *C*: nondiabetic animals, 2.1-mm defect; *D*: diabetic animal, 1.0-mm bone defect; *E*: diabetic animal, 1.6-mm bone defect; *F*: diabetic animals, 2.1-mm defect. Bar = 0.1 mm.

wt. of 62.5 mg/ml ketamine hydrochloride (Ketalar; Parke-Davis, Morris Plains, NJ) and 6.25 mg/ml xylazine (Rompum; Mobay, Shawnee, KS). Initial experiments investigating the effect of diabetes on bone healing used circular craniotomy defects of 1.0-, 1.6-, or 2.1-mm diameter prepared in parietal bones of diabetic and nondiabetic animals with cylindrical low-speed carbide burs (Nos. 2011, 2016, 2021; Meissinger, Dusseldorf, Germany) and saline irrigation. Subsequent experiments used 1-mm defects. As an analgesic after surgery, animals were given buprenorphine (Temgesic 0.3 mg/ml, i.p.; Reckitt & Collman, Hull, U.K.) 3 mg/kg twice a day for 3 days. In all, <2% of animals showed clinical signs of infection; the infected animals were excluded from the study. Animals were killed by CO_2 asphyxiation 14 days after the surgical procedures. Heads were processed for histology and quantitative histomorphometric analyses. This time point was chosen based on time studies of healing craniotomy defects in rats (36,37).

CML-albumin application to defects in nondiabetic animals. Four groups of six nondiabetic animals each (n = 6) were used to determine whether CML-albumin applied by surgically implanted osmotic mini-pumps inhibited bone formation compared to unmodified albumin. The four groups of animals received 90 or 900 μg of control mouse serum albumin (MSA) or CML-modified MSA continuously applied over the 2-week experimental period. Circular craniotomy defects (1.0-mm diameter) were prepared in the parietal bones. This defect size was chosen because bone healing is normally complete in 14 days in nondiabetic animals (Fig. 1), and it allowed the determination of inhibitory effects of locally applied substances. Alzet mini-pumps were placed in dermal pouches created in the backs of animals and did not remain exposed after surgical procedures. The pump catheter end was positioned with the aperture being located slightly over the edge of the bone defect, and glued in place with cyanoacrylate. Animals were killed 14 days after the surgical procedure.

CML-MSA was prepared by chemical modification from highly purified MSA (Calbiochem), as previously described (20). Products were chromatographed through a Detoxi-Gel affinity column (Pierce). The final concentration of the CML-MSA and control MSA was 9 mg/ml. Endotoxin levels were <2.5 pg/ml (E-Toxate kit; Sigma). In total, 30% of lysine residues in CML-MSA were converted to CML, as determined by the TNBS (trinitrobenzenesulfonic acid) assay and consistent with previous studies (20,38). CML-MSA was highly reactive on Western blots with anti-CML monoclonal antibody 6D12 (Waako) (32,39), whereas control MSA was not reactive.

Histology and analyses. Block biopsies were prepared and specimens were fixed in 10% buffered formalin at 4°C, decalcified in EDTA for 5–7 days, dehydrated, and embedded in paraffin. Serial sections (4 μm) were stained with hematoxylin and eosin. The three most central sections of each defect were analyzed. Linear measurements obtained with an image analysis system (Image-Pro Plus 4.0; Media Cybernetics, Silver Spring, MD). Bone bridging was expressed as a percentage of the total defect width. Measurements included *1*) the distance between the rims of the initial bone defect and *2*) the distance between the rims of the remaining defect, and the percent bone bridging was calculated. The area of regenerated bone was measured from digitally captured images using ImagePro 4.0 software.

Immunohistochemistry. The expression of RAGE was determined in diabetic and nondiabetic healing defects by quantitative immunohistochemical analyses of six animals per group in a separate experiment. Defects (1-mm diameter) were created as described above on day 19 in diabetic and nondiabetic control animals. Block biopsies were taken 10 days after the surgical procedure. A time point of 10 days of healing was selected because we wished to evaluate tissues during active healing in both diabetic and nondiabetic animals. Specimens were fixed in 4% paraformaldehyde for 18 h, decalcified in EDTA for 5–7 days, and placed in 10% sucrose overnight at 4°C. Samples were then stored in 2-methylbutane at −80°C. The specimens were embedded in Tissue Prep (Fisher Scientific), after which 6-μm cryosections were mounted on ProbeOn Plus slides (Fisher Scientific) and stored at −80°C until staining. Immunostaining was performed using the immunoperoxidase/diaminobenzidine technique (avidin-biotin-horseradish peroxidase complex−Vectastain complex kit Elite; Vector Laboratories), according to the manufacturer's protocols. RAGE antiserum was generously provided by Merck (40). Slides were counterstained with hematoxylin. Quantitative histo-

morphometric analyses were carried out, with three central sections being measured for each bone defect; five nonoverlapping fields were measured per slide at 400× magnification. The total surface area per field was 420 μm^2. The total number of RAGE positive cells was counted in each of the three anatomical areas of interest: the periosteum, the dura mater, and the granulation tissue filling the healing bone defect.

RT-PCR and Western blots for RAGE in osteoblasts. Total RNA was isolated from MC3T3-E1 cells cultured in Dulbecco's modified Eagle's medium containing 10% FCS and antibiotics using TRIzol (Gibco/BRL). polyA + RNA was isolated (Qiagen Oligotex mRNA spin column). RT was performed on 6 μg polyA + mRNA using a RAGE-specific anti-sense primer (GTATCAAATGT TACTCAG) and a Superscript II kit (Promega). PCR was then performed on aliquots with primer sets A and B. Primer set A flanks intron 2 of RAGE and will produce a 194-bp cDNA from RAGE mRNA; primer set B flanks intron 7 and should produce a 159-bp cDNA from RAGE mRNA or a 326-bp product from RAGE genomic DNA. The sequences of primer set A are TTGGAGAGC CACTTGTGCTA (forward) and CCCTCATCGACAATTCCAGT (reverse); for primer set B, they are TCCACTGGATAAAGGATGGTG (forward) and GAC CCTGATGCTGACAGGAG (reverse). PCR cycling parameters were 30 cycles—94°C, 30 s; 60°C, 45 s; and 72°C 1 min—and buffer contained 1.5 mmol/l $MgCl_2$.

Western blots for RAGE were performed on SDS-PAGE sample buffer extracts of MC3T3-E1 cells and cultures of primary rat osteoblasts (41). Goat anti-RAGE antiserum (1:1,000) (40) or nonimmune goat antiserum were used as primary antibodies, and bands were visualized with alkaline phosphatase-coupled rabbit anti-goat IgG and Western Blue substrate (Promega).

Statistics. Biochemical measurements were analyzed with the Student's t test for ordinal variables and with the Wilcoxon's signed-rank test for cardinal variables. Histomorphometric measurements for bone area determinations were analyzed with Student's t test, whereas those for bone bridging were analyzed with Wilcoxon's signed-rank test. Analyses of immunohistochemistry studies of positively stained cells for RAGE were performed with a t test for independent samples. Histomorphometric measurements for bone area and bone bridging on defects treated with exogenous application of MSA or CML-MSA were analyzed with one-way ANOVA. Post hoc statistical testing was performed using a t test for independent groups and Wilcoxon's signed-rank test. A value of 95% or higher for α was used to declare statistical significance for the studies reported.

RESULTS

Experiments were performed to determine if type 1 diabetes results in diminished bone healing. The multiple low-dosage STZ mouse model was chosen because the level of hyperglycemia is comparable to that in human type 1 diabetes (35). Three different calvaria defect sizes were evaluated in diabetic and nondiabetic animals to investigate whether diabetes influences healing in bone lesions normally capable of full healing in 14 days and in larger defects. For these studies, 36 animals were divided into six groups, three diabetic and three nondiabetic, with 6 animals in each group.

Diabetes induction and characterization. Twice weekly monitoring of blood and urine glucose levels indicated that diabetes developed by day 12, reaching the threshold level of 250 mg glucose/dl, in all animals receiving STZ, and did not develop in control animals, as expected. The metabolic measurements summarized in Table 1 demonstrate that the diabetic state of animals occurred without unexpected complications. Glucose measurements in urine confirmed blood glucose measurements. Twice weekly assays for the presence of ketones and protein were below detectable levels as expected for diabetes without ketoacidosis and kidney complications. GHb levels measured on day 33 (Table 1) were elevated in diabetic animals (42). These data indicated that hyperglycemia was consistent and not transient. Food intake was elevated in diabetic animals, whereas animal weight was reduced by ~10%; this indicated the presence of hyperphagia accompanied by modest weight loss, as expected (43), and not unexpected metabolic dysregulation. Weight loss in diabetic animals occurred during diabetes onset until day 11, and weight gain then resumed at a normal rate for the rest of the experimental period (days 12–33). Insulin levels in serum were reduced in diabetic animals, as expected (Table 1) (42).

TABLE 1
Biochemical evaluation and quantification of the body weight and food intake of nondiabetic and diabetic animals

Parameter	Nondiabetic	Diabetic
Blood glucose (mg/dl)	125.55 ± 23.22	385.50 ± 54.53*
Urine glucose (mg/dl)	None detected	500
Insulin (ng/ml)	0.73 ± 0.03	0.50 ± 0.06*
GHb (%)	6.6 ± 0.6	13.4 ± 1.2*
Protein (urine)	0	0
Ketones (urine)	0	0
Food ($g \cdot day^{-1} \cdot animal^{-1}$)	7.2 ± 2.3	12.3 ± 1.4*
Weight (g)	28.2 ± 0.25	25.8 ± 0.3*

Data are n or means ± SD. Measurements were obtained after animals were killed on day 33, except for food consumption which was monitored twice per week throughout the experimental period. Glucose, urine protein and ketone levels, food consumption, and weight measurements were obtained from 25 animals per group; insulin and GHb measurements were obtained from 8 animals per group. *$P < 0.05$, by unpaired t or Mann-Whitney test.

On experimental day 19, 7 days after the onset of diabetes, circular craniotomy defects with diameters of 1.0, 1.6, or 2.1 mm were created in diabetic and nondiabetic animals as described above, resulting in six groups of animals. Animals were killed after 14 days of healing (day 33) (36,37). Histologic evaluation of healed lesions revealed that bone formation was more abundant in nondiabetic animals than in the diabetic animals for all three lesions sizes (Fig. 1*A–C* [normal] versus *D–F* [diabetic]). Intense osteoblastic activity was seen in the growing osteogenic fronts, in both the periosteal and dural surfaces. Woven bone was observed within the lesion extending toward most of the linear dimension of the defects in normal animals. Marrow cavities had formed and numerous osteocytes were embedded in the bone matrix. By contrast, more limited bone formation was seen in diabetic animals. Marrow spaces appeared less developed and fibrous connective tissue with low amounts of cellular and vascular structures filled the bone defect.

Linear and surface area histomorphometric evaluations demonstrated that bone healing was inhibited in diabetic animals (Fig. 2). Both bone bridging and the area of bone formed were significantly inhibited compared to normal controls (Fig. 2). In normal animals, defects of 1.0-mm diameter were healed almost completely (92% bone bridging), and defects of 1.6- and 2.1-mm diameter exhibited partial healing (Fig. 2*A*). The healing in larger defects was characterized by discrete osteogenesis and predominant soft tissue closure. Interestingly, bone bridging in diabetic animals was inhibited by ~40% compared with that of normal animals for all the defect sizes tested. These results demonstrated that bone healing is significantly and consistently diminished in diabetic animals.

Insulin treatment rescued inhibited bone healing in diabetic animals. An experiment was performed to determine whether the observed diminished bone healing

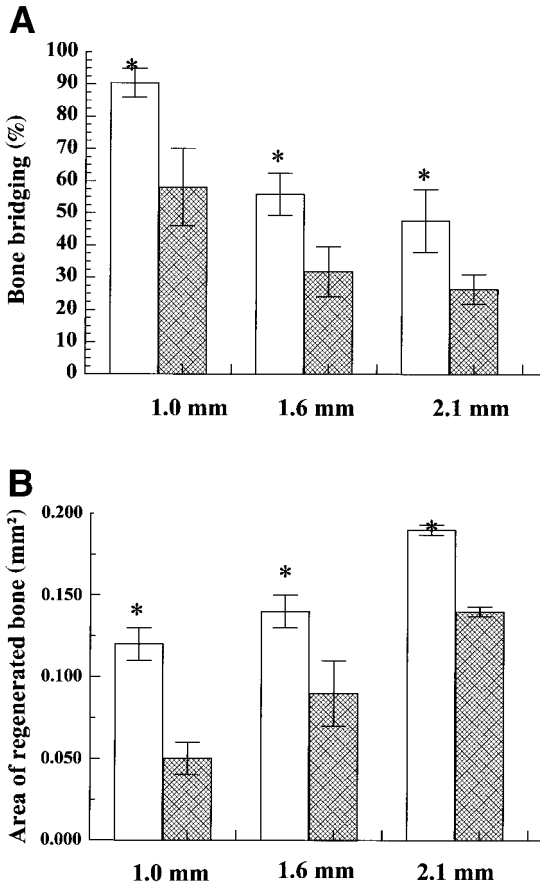

FIG. 2. Histomorphometric analyses of healed calvarial bone defects from diabetic (▨) and nondiabetic (□) animals after 14 days of healing. *A*: Bone bridging measurements. Linear measurements of bone ingrowth from the rims of the initial defects toward its center was quantified after 14 days of healing in three center sections per specimen. Bone bridging was expressed as a percent of the total defect width. *B*: Area of regenerated bone. Area of regenerated bone was measured from digitally captured images of stained slides made from three center sections per specimen. Boundaries of the features of interest were traced with a mouse-driven cursor on video images on the display monitor with a hand-held mouse. The area of the outlined image was then calculated electronically with the software package. Bone area was measured in three slides for each bone defect from each animal. The readings were averaged to obtain means for each bone defect, and both defects were averaged to obtain the mean for every animal, which was then used as the unit for statistical analyses. Results were presented as means ± SE. Data reported were obtained from 18 diabetic and 18 normal animals. *$P < 0.05$ by unpaired t or Mann-Whitney test.

was attributable to insulin deficiency. A control and test group were formed with diabetic animals ($n = 7$ in each group). The test animals received daily insulin injections and the control animals received daily saline injections. Daily insulin injections (10 IU/kg, i.p.) began immediately after the onset of hyperglycemic diabetic status (day 12). Then 7 days later, 1-mm circular craniotomy defects were created in the parietal bones. The efficacy of insulin treatment and dosage was determined by daily urine glucose measurements and by determination of GHb levels when the animals were killed on day 33. GHb levels in blood from insulin-treated animals were lower than those in untreated animals (8.36 ± 1.95 vs. 11.35 ± 1.03%, respectively; $P < 0.0001$), supporting the observation that insulin administration consistently reduced blood glucose levels, as expected.

Histology of healed lesions after 14 days of healing (day 33) revealed that bone formation was more abundant in diabetic animals treated with insulin than in untreated diabetic animals (Fig. 3*B*). Osteoblastic activity was seen in both the periosteal and dural surfaces. Woven-like bone was present within the lesion extending through most of the linear dimension of the defects. Marrow cavities were formed and numerous osteocytes were embedded in the bone matrix. Significant cellular and vascular activity occurred in the connective tissue surrounding the newly formed bone. Less bone formation was seen in diabetic animals not treated with insulin (Fig. 3*A*).

Linear and surface area histomorphometric evaluations of histologic slides demonstrated that bone healing was rescued in diabetic animals treated with insulin. Defects from insulin-treated diabetic animals exhibited significantly more bone bridging than the defects from control diabetic animals (84.81 ± 12.24 vs. 62.26 ± 24.76%; $P = 0.001$) (Fig. 3*C*). Results from bone area measurements paralleled those from bone bridging measurements. Defects from control diabetic animals exhibited significantly less regenerated bone than defects from insulin-treated diabetic animals (0.06 ± 0.04 vs. 0.14 ± 0.04 mm^2; $P = 0.001$) (Fig. 3*D*). These data provide direct evidence that the alterations in bone healing observed in our model resulted from the consequences of insulin deficiency and hyperglycemia rather than from potential secondary effects of STZ.

RAGE expression in vivo. RAGE mediates many of the effects of AGEs in different cell types. To our knowledge, RAGE expression has not been linked to altered bone formation or healing. The localization and quantitation of RAGE was, therefore, determined in healing calvaria defects in diabetic and nondiabetic animals by immunoperoxidase methodology with a specific goat anti-RAGE primary antibody. The data demonstrated higher levels of RAGE in calvarial tissues of diabetic animals (Fig. 4*B* and *E*), with low, but still detectable levels of RAGE staining observed in nondiabetic tissues (Fig. 4*A* and *E*). In diabetic tissues, positive-stained cells with morphology consistent with that of mesenchymal cells were observed in the dura mater, periosteum, and nonmineralized granulation tissue filling the bone defect (Fig. 4*B*). Mononuclear cuboidal and fusiform mesenchymal cells associated with the bone on the growing osteogenic front were also positively stained (Fig. 4*B*), suggesting that osteoblasts and pre-osteoblasts may overexpress RAGE. RAGE staining was observed in cells distant from calvaria defects, suggesting that wounding is not required for increased RAGE expression in diabetic calvaria. Multinucleated cells adjacent to bone staining for RAGE were not observed, suggesting that increased osteoclast activation in diabetes probably was not occurring after 14 days of healing. Taken together, the results demonstrated that RAGE is upregulated in fibrogenic cells in calvaria of diabetic animals.

Exogenous application of AGEs to nondiabetic lesions. Because of the presence of RAGE in healing calvaria, it was hypothesized that AGEs could contribute to diminished bone healing in diabetes via AGE-RAGE interactions. Experiments were performed to determine whether a locally applied RAGE ligand could inhibit intramembranous bone healing in normal (nondiabetic)

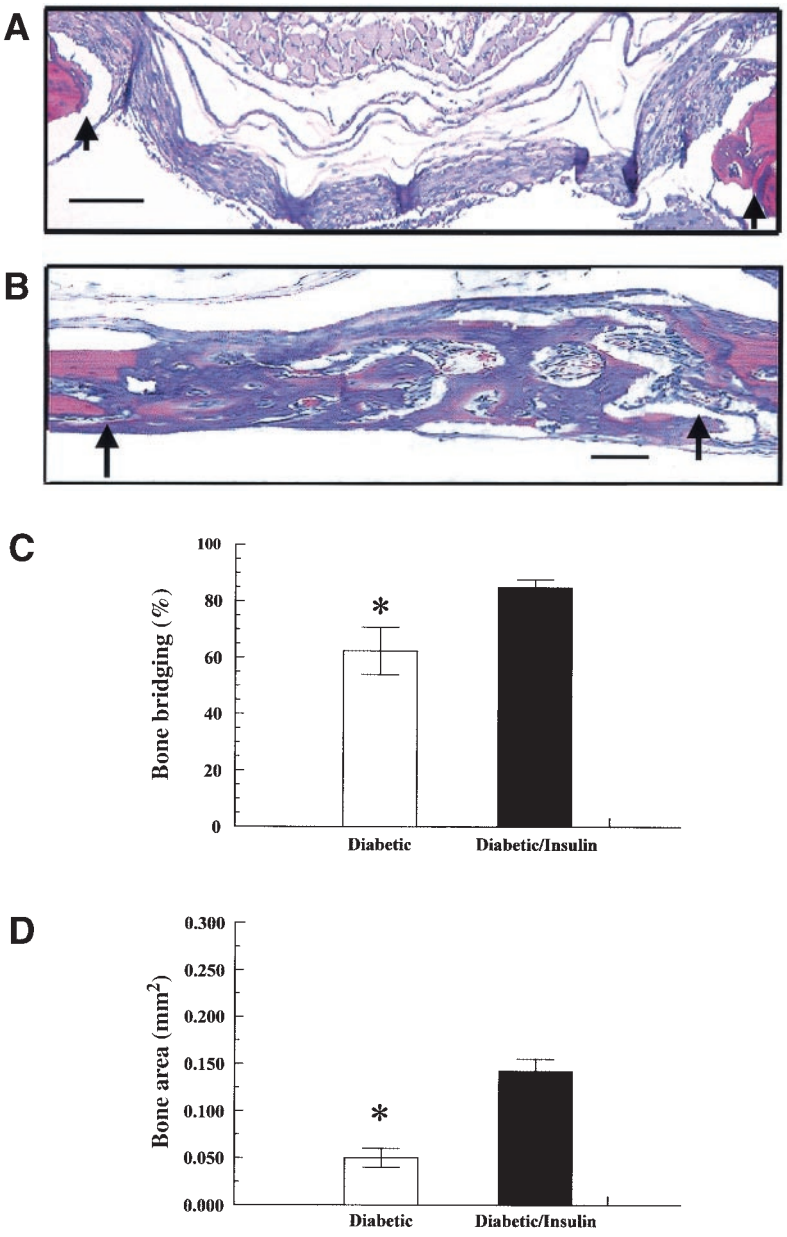

FIG. 3. Histology showing rescue of diminished bone healing in diabetic animals by insulin treatment (*A*, saline-treated; *B*, insulin-treated) and histomorphometric analyses (*C* and *D*) of animals treated with saline (□) or insulin (■). Standardized bone defects of 1.0-mm diameter were created in the calvaria of 14 diabetic animals. Half of the animals were treated with daily injections of insulin immediately after diabetes onset. All the animals were killed after 14 days of healing. In *A* and *B*, representative slides from decalcified specimens stained with hematoxylin and eosin are shown. Black arrows indicate margins of the original bone defect; bars indicate 0.1 mm. In *C* and *D*, data are means ± SE. Results presented are from seven saline-treated and seven insulin-injected diabetic animals. **P* = 0.001 by unpaired *t* or Mann-Whitney test.

animals. MSA was modified to contain biologically active levels of CML, a known RAGE ligand (20). Continuous local delivery of CML-MSA or MSA over 14 days to calvaria defects was accomplished with surgically implanted Alzet mini-pumps. Unilateral craniotomy defects were created in nondiabetic animals for this experiment. All the animals were killed 14 days after the surgical procedure.

Histologic evaluation of control MSA-treated lesions demonstrated woven bone within the lesion extending through most of the linear dimension of the defects (Fig. 5*A* and *B*). Osteoblastic activity was seen in the growing osteogenic fronts in both the periosteal and dural surfaces. Well-developed marrow cavities with numerous osteocytes were embedded in the bone matrix. Significant cellular and vascular activity was seen in the connective tissue surrounding the newly formed bone. By contrast, bone formation was significantly inhibited in defects treated with CML-MSA and resembled diabetic lesions in histologic appearance (Fig. 5*C* and *D*).

Histomorphometric analyses revealed that bone defects receiving MSA healed almost completely. Application of CML-MSA to 1.0-mm craniotomy defects in normal animals resulted in inhibition of bone formation (Fig. 5*E*). A dosage-response effect was noted for the two dosages of CML-MSA tested; the higher dosage resulted in significantly more inhibition of bone healing than the lower dosage. These alterations were independent of sustained hyperglycemia, as expected, as levels of GHb were normal and essentially the same as in the nondiabetic blood samples shown in Table 1.

RAGE in cultured osteoblasts. It has been suggested that there is a pathway by which AGEs interact with cell surface receptors, leading to altered osteoblast function (44–46). Our data suggest that RAGE in particular may contribute to AGE modulation of osteoblast function. It is notable that RAGE expression in osteoblasts has not been previously reported. We wished to determine whether phenotypically normal murine osteoblastic MC3T3 cells

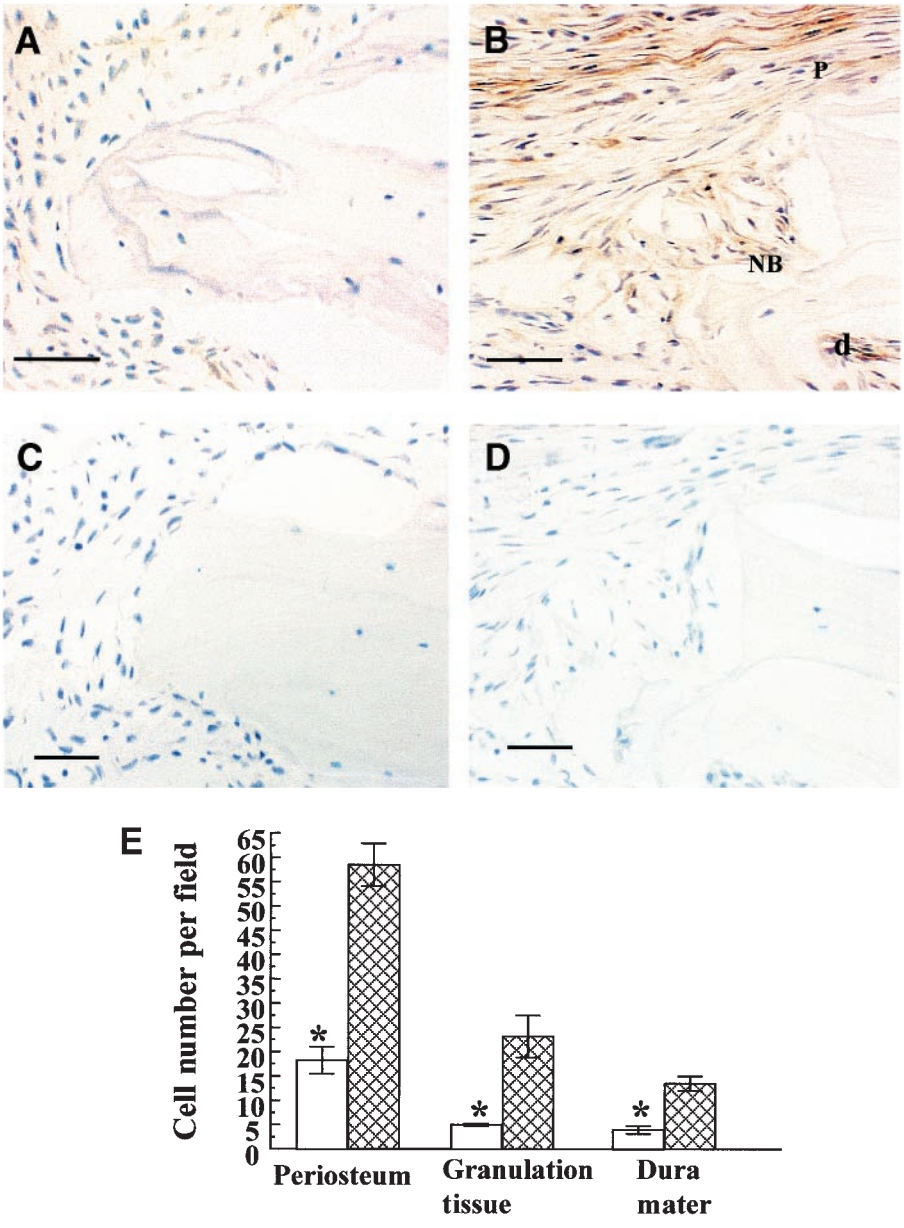

FIG. 4. Immunohistochemistry for RAGE (*A–D*) and histomorphometric analyses (*E*). Diabetic and nondiabetic animals were killed after 10 days of healing, and frozen sections of the defect area were prepared ($n = 6$). Immunostaining for RAGE was performed using goat anti-RAGE antiserum and bound antibody visualized by immunoperoxidase secondary reagents (see RESEARCH DESIGN AND METHODS). Slides were counterstained with hematoxylin. Magnification shown 400×. *A* and *B*: Nondiabetic (*A*) and diabetic (*B*) calvaria showing positive staining of periosteum (p), margin of defect (nb), and in the dura mater (d). *C* and *D*: Nonimmune control of nondiabetic (*C*) and diabetic (*D*) tissue. Bar = 0.06 mm. *E*: positive cells per field in three slides per specimen at a magnification of 400× were determined in five nonoverlapping fields each in the periosteum, granulation tissue in the center of the defects, and dura mater, as described in RESEARCH DESIGN AND METHODS. □, control nondiabetic specimens; ▨, diabetic specimens. Unpaired *t* test or Mann-Whitney test were used for statistical analyses. α ≥95% was used to declare statistical significance.

expressed RAGE mRNA and protein. Murine RAGE cDNA and genomic sequences were obtained to permit design of RT-PCR primers for assessment of RAGE mRNA. BLAST searches of murine Expressed Sequence Tag databases were performed against the published rat RAGE cDNA sequence identified murine cDNAs, with 98% similarity to the rat sequence (e.g., accession number AA882247). BLAST searches of the murine cDNA sequence against murine genomic databases identified the RAGE gene sequence on mouse chromosome 17 (accession numbers AC006289 and MMHC29N7). Exon/intron sequences and organization were identified and two RT-PCR primer pairs were designed that flank introns 2 and 7 (primer sets A and B, respectively; see RESEARCH DESIGN AND METHODS). As is shown in Fig. 6*A*, both primer sets in RT-PCR reactions of total RNA from murine MC3T3 cells produced PCR products consistent with the presence of RAGE mRNA. RT-PCR products were cloned and sequenced and found to be identical to the expected sequences for murine RAGE cDNAs. Thus murine MC3T3 osteoblasts express RAGE mRNA.

To determine the presence of RAGE protein in osteoblasts, SDS-PAGE sample buffer extracts of MC3T3 cells and primary rat osteoblast cultures were assayed by Western blotting using anti-RAGE antiserum. As shown in Fig. 6*B*, extracts made from MC3T3 cells and primary rat osteoblasts contained a specific immunoreactive band at ~50 kDa, consistent with the presence of full-length RAGE protein (47).

DISCUSSION

Osteopenia is a complication of diabetes in humans (4–6,11–14). Evidence for reduced osteoblastic activity and osteopenia has been reported in type 1 diabetes (11–14,48,49). The results of the present studies indicate that type 1 diabetes impairs intramembranous bone healing, as demonstrated by our finding that the degree of healing of circular osteotomies was reduced by 40% in diabetic

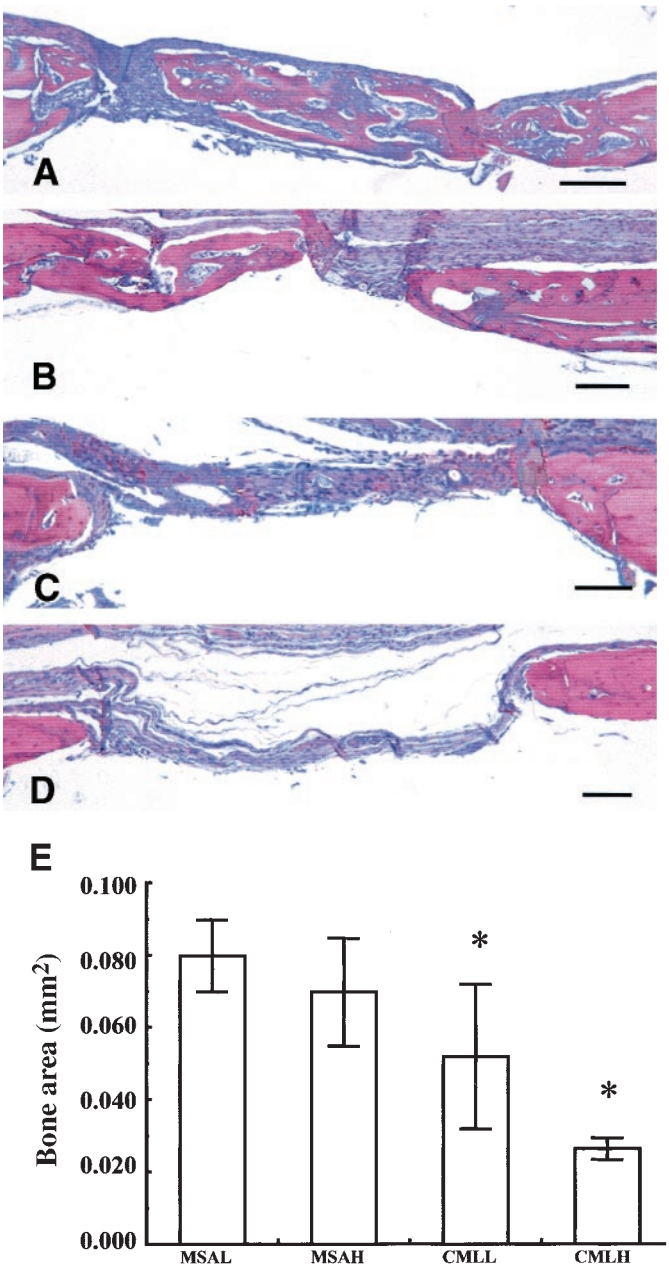

FIG. 5. Histology of defects with local application of 90 μg MSA (*A*), 0.9 mg MSA (*B*), 90 μg CML-MSA (*C*), or 900 μg CML-MSA (*D*) and histomorphometric analyses (*E*). *A*–*D*: Hematoxylin and eosin stain, 100× magnification, bar = 0.1 mm. *E*: Area of regenerated bone. Serial sections (4 μm) were cut through the specimens and stained with hematoxylin and eosin. Representative specimens of the center of the defects were analyzed at 100× magnification. Area of regenerated bone was measured from digitally captured images of stained slides. Boundaries of the features of interest were traced with a mouse-driven cursor on video images on the display monitor with a hand-held mouse. The area of the outlined image was then calculated electronically with the software package. Bone area was measured in three slides for each bone defect from each animal, with six animals per experimental group (n = 6). The readings were averaged to obtain means for each bone defect, and both defects were averaged to obtain the mean for every animal, which was then used as the unit for statistical analyses. Results are presented as means ± SE. *P < 0.05 by Student's t or Mann-Whitney test.

animals versus nondiabetic controls. To rule out other complications that could potentially arise from STZ treatment, a diabetic group was treated with insulin. Insulin treatment largely restored healing, indicating that the impaired healing was strictly related to the diabetic state.

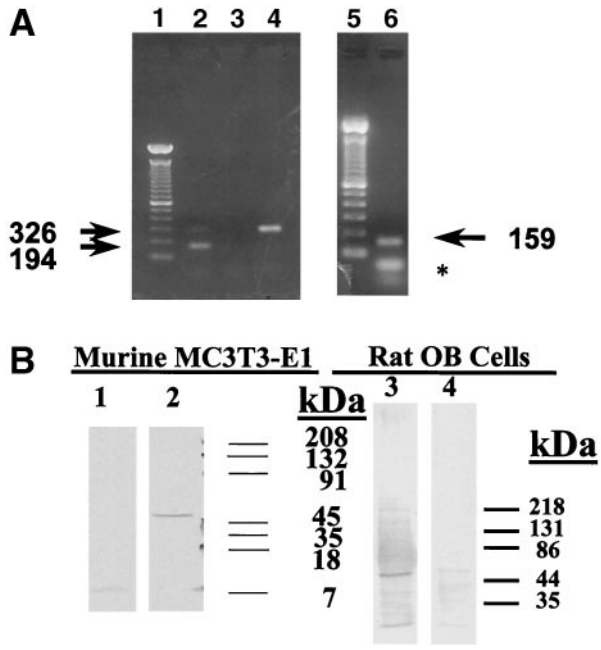

FIG. 6. Ethidium bromide–stained agarose gel of RT-PCR products of MC3T3-E1 RNA (*A*) and Western blot assay for RAGE protein in MC3T3-E1 cells and in primary rat osteoblast cells extracts (*B*). *A*: *Lane 1*, 100-bp ladder; *lane 2*, expected 194-bp RT-PCR product from RNA using primer set A (flanking intron 2); *lane 3*, no template control PCR; *lane 4*, PCR of murine genomic DNA from primer set A (flanking intron 2) showing predicted 326-bp product; *lane 5*, 100-bp ladder; *lane 6*, RT-PCR product from MC3T3-E1 RNA using primer set B (flanking intron 7) showing predicted 159-bp product. PCR reactions contained 1.5 mmol/l $MgCl_2$ and the annealing temperature was 60°C. PCR was carried out for 30 cycles. *Position of primer/dimers. *B*: MC3T3 cells and primary rat osteoblast cells were grown as described. Cell layers of confluent cultures were extracted into SDS-PAGE sample buffer, and aliquots containing 100 μg of protein were subjected to 10% SDS-PAGE under reducing conditions and then transferred and subjected to Western blotting. Goat anti-RAGE anti-serum or nonimmune goat serum were used at a dilution of 1:1,000. *Lane 1*, nonimmune goat serum; *lane 2*, anti-RAGE; *lane 3* anti-RAGE; *lane 4*, nonimmune goat serum.

Biochemical and immunohistochemical studies indicate that CML-modified proteins are AGEs that accumulate in vivo in diabetes (20,30–34). The identification of these modifications as unique AGE species with the capacity to bind RAGE suggests a mechanism by which the engagement of RAGE by CML-proteins results in diabetic complications (20). In vitro studies have shown that murine osteoblastic cells possess receptors that bind AGEs, although RAGE itself has not been identified (50). We have reported here that osteoblasts do express RAGE mRNA and protein. To investigate the role of diabetes in RAGE expression in bone, immunohistochemical studies were carried out in healing osseous wounds in normal and diabetic mice. RAGE expression was detected in the nondiabetic mice and was significantly upregulated in diabetic animals. RAGE expression was noted in cells associated with bone-forming activity, suggesting that enhanced expression could affect osseous healing.

Further evidence for a pathologic role of AGE interactions in the inhibited bone healing observed was obtained by determining whether controlled local application to defects of a known RAGE ligand, CML-MSA, could inhibit healing in normal animals and mimic deficient healing observed in diabetic animals. The application of CML-MSA to craniotomy defects significantly impaired healing by at

least 40% compared to animals treated with unmodified control MSA, which is not a ligand for RAGE. In future studies, it will be interesting to determine the effects on bone healing of CML extracellular matrix proteins modified to contain varying amounts of CML; this will allow us to assess the effects of more physiologically important bone proteins modified with more physiological levels of CML. It should be noted that the 30% of the lysine residues in the modified albumin used in the present study were CML residues.

Systemic injections of AGEs result in pathologic alterations, similar to the typical consequences of diabetes (51,52), and AGE accumulation in target tissues is pathogenic (30–34). CML residues are AGE antigens (30–34) and are linked to the pathogenesis of functional tissue damage in complications of diabetes (20). The finding that locally applied CML-MSA impairs osseous healing is consistent with the concept that formation of AGEs during chronic hyperglycemia represents a critical event that contributes to defective bone healing in type 1 diabetes. Moreover, this interpretation is supported by recent findings that AGE adducts inhibit osteoblast differentiation and may contribute to bone disease in part by altering the response to parathyroid hormone (50,53). The observations in the present study directly identify the increased presence of RAGE in healing diabetic bone and RAGE expression in osteoblast cultures. Moreover, the finding that biological activity of CML-MSA in inhibiting bone healing and formation in vivo mimics the effect of diabetes further supports the notion that AGEs inhibit osteoblast function and contribute to diabetic bone disease. Our results may have relevance to the mechanistic basis for increased alveolar bone loss in diabetic mice with periodontal disease (19). We speculate that AGE-RAGE interactions on osteoblastic cells inhibit osteoblast function and contribute to diminished bone formation. Further studies linking diabetic osteopenia to AGEs and osteoblast function are envisioned.

ACKNOWLEDGMENTS

This research was supported by National Institutes of Health Grants DE-12209 and DE-14066 (to P.C.T.), DE-12482 and DE-14079 (to S.A.), and DE-13191 (to D.T.G.), and a CAPES Fellowship (Brazil) to R.B.S.

The authors are grateful to Drs. Michael Neeper, Allan Shaw, and Emilio Emini of Merck & Co., West Point, PA for the gift of goat anti-RAGE antiserum. We thank Dr. Yasuo Ido of Boston University School of Medicine for valuable advice regarding management of diabetic mice, and Dr. Wayne Gonnerman of Boston University for expert technical assistance.

REFERENCES

1. De Leeuw I, Abs R: Bone mass and bone density in maturity-type diabetics measured by the ^{125}I photon-absorption technique. *Diabetes* 26:1130–1135, 1977
2. Heath H 3rd, Lambert PW, Service FJ, Arnaud SB: Calcium homeostasis in diabetes mellitus. *J Clin Endocrinol Metab* 49:462–466, 1979
3. McNair P, Madsbad S, Christiansen C, Faber OK, Transbol I, Binder C: Osteopenia in insulin treated diabetes mellitus: its relation to age at onset, sex and duration of disease. *Diabetologia* 15:87–90, 1978
4. Levin ME, Boisseau VC, Avioli LV: Effects of diabetes mellitus on bone mass in juvenile and adult-onset diabetes. *N Engl J Med* 294:241–245, 1976
5. Santiago JV, McAlister WH, Ratzan SK, Bussman Y, Haymond MW, Shackelford G, Weldon VV: Decreased cortical thickness and osteopenia in children with diabetes mellitus. *J Clin Endocrinol Metab* 45:845–848, 1977
6. Seino Y, Ishida H: Diabetic osteopenia: pathophysiology and clinical aspects. *Diabetes Metab Rev* 11:21–35, 1995
7. Levy J, Reid I, Halstad L, Gavin JR, Avioli LV: Abnormal cell calcium concentrations in cultured bone cells obtained from femurs of obese and noninsulin-dependent diabetic rats. *Calcif Tissue Int* 44:131–137, 1989
8. Cozen L: Does diabetes delay fracture healing? *Clin Orthop* 82:134–140, 1972
9. Bouillon R, Bex M, Van Herck E, Laureys J, Dooms L, Lesaffre E, Ravussin E: Influence of age, sex, and insulin on osteoblast function: osteoblast dysfunction in diabetes mellitus. *J Clin Endocrinol Metab* 80:1194–1202, 1995
10. Bouillon R: Diabetic bone disease: low turnover osteoporosis related to decreased IGF-I production. *Verh K Acad Geneeskd Belg* 54:365–391, 1992
11. Aubia J, Serrano LI, Marinoso L, Hojman L, Diez A, Lloveras J, Masramon J: Osteodystrophy of diabetics in chronic dialysis: a histomorphometric study. *Calcif Tissue Int* 42:297–301, 1988
12. Rico H, Hernandez ER, Cabranes JA, Gomez-Castresana F: Suggestion of a deficient osteoblastic function in diabetes mellitus: the possible cause of osteopenia in diabetics. *Calcif Tissue Int* 45:71–73, 1989
13. Shore RM, Chesney RW, Mazess RB, Rose PG, Bargman GJ: Osteopenia in juvenile diabetes. *Calcif Tissue Int* 33:455–457, 1981
14. Krakauer JC, McKenna MJ, Buderer NF, Rao DS, Whitehouse FW, Parfitt AM: Bone loss and bone turnover in diabetes. *Diabetes* 44:775–782, 1995
15. Brownlee M, Cerami A, Vlassara H: Advanced products of nonenzymatic glycosylation and the pathogenesis of diabetic vascular disease. *Diabetes Metab Rev* 4:437–451, 1988
16. Brownlee M, Cerami A, Vlassara H: Advanced glycosylation end products in tissue and the biochemical basis of diabetic complications. *N Engl J Med* 318:1315–1321, 1988
17. Ruderman NB, Williamson JR, Brownlee M: Glucose and diabetic vascular disease. *FASEB J* 6:2905–2914, 1992
18. Lalla E, Lamster IB, Feit M, Huang L, Schmidt AM: A murine model of accelerated periodontal disease in diabetes. *J Periodontal Res* 33:387–399, 1998
19. Lalla E, Lamster IB, Feit M, Huang L, Spessot A, Qu W, Kislinger T, Lu Y, Stern DM, Schmidt AM: Blockade of RAGE suppresses periodontitis-associated bone loss in diabetic mice. *J Clin Invest* 105:1117–1124, 2000
20. Kislinger T, Fu C, Huber B, Qu W, Taguchi A, Du Yan S, Hofmann M, Yan SF, Pischetsrieder M, Stern D, Schmidt AM: N(epsilon)-(carboxymethyl) lysine adducts of proteins are ligands for receptor for advanced glycation end products that activate cell signaling pathways and modulate gene expression. *J Biol Chem* 274:31740–31749, 1999
21. Kislinger T, Tanji N, Wendt T, Qu W, Lu Y, Ferran LJ Jr, Taguchi A, Olson K, Bucciarelli L, Goova M, Hofmann MA, Cataldegirmen G, D'Agati V, Pischetsrieder M, Stern DM, Schmidt AM: Receptor for advanced glycation end products mediates inflammation and enhanced expression of tissue factor in vasculature of diabetic apolipoprotein E-null mice. *Arterioscler Thromb Vasc Biol* 21:905–910, 2001
22. Schmidt AM, Yan SD, Yan SF, Stern DM: The biology of the receptor for advanced glycation end products and its ligands. *Biochim Biophys Acta* 1498:99–111, 2000
23. Baynes JW, Watkins NG, Fisher CI, Hull CJ, Patrick JS, Ahmed MU, Dunn JA, Thorpe SR: The Amadori product on protein: structure and reactions. *Prog Clin Biol Res* 304:43–67, 1989
24. Skolnik EY, Yang Z, Makita Z, Radoff S, Kirstein M, Vlassara H: Human and rat mesangial cell receptors for glucose-modified proteins: potential role in kidney tissue remodelling and diabetic nephropathy. *J Exp Med* 174:931–939, 1991
25. Vlassara H, Brownlee M, Cerami A: Specific macrophage receptor activity for advanced glycosylation end products inversely correlates with insulin levels in vivo. *Diabetes* 37:456–461, 1988
26. Baynes JW: Role of oxidative stress in development of complications in diabetes. *Diabetes* 40:405–412, 1991
27. Yan SD, Schmidt AM, Anderson GM, Zhang J, Brett J, Zou YS, Pinsky D, Stern D: Enhanced cellular oxidant stress by the interaction of advanced glycation end products with their receptors/binding proteins. *J Biol Chem* 269:9889–9897, 1994
28. Schmidt AM, Hori O, Cao R, Yan SD, Brett J, Wautier JL, Ogawa S, Kuwabara K, Matsumoto M, Stern D: RAGE: a novel cellular receptor for advanced glycation end products. *Diabetes* 45 (Suppl. 3):S77–S80, 1996
29. Lalla E, Lamster IB, Schmidt AM: Enhanced interaction of advanced glycation end products with their cellular receptor RAGE: implications for the pathogenesis of accelerated periodontal disease in diabetes. *Ann Periodontol* 3:13–19, 1998

30. Berg TJ, Clausen JT, Torjesen PA, Dahl-Jorgensen K, Bangstad HJ, Hanssen KF: The advanced glycation end product N epsilon-(carboxymethyl)lysine is increased in serum from children and adolescents with type 1 diabetes. *Diabetes Care* 21:1997–2002, 1998
31. Dunn JA, McCance DR, Thorpe SR, Lyons TJ, Baynes JW: Age-dependent accumulation of N epsilon-(carboxymethyl)lysine and N epsilon-(carboxymethyl)hydroxylysine in human skin collagen. *Biochemistry* 30:1205–1210, 1991
32. Ikeda K, Higashi T, Sano H, Jinnouchi Y, Yoshida M, Araki T, Ueda S, Horiuchi S: N (epsilon)-(carboxymethyl)lysine protein adduct is a major immunological epitope in proteins modified with advanced glycation end products of the Maillard reaction. *Biochemistry* 35:8075–8083, 1996
33. Reddy S, Bichler J, Wells-Knecht KJ, Thorpe SR, Baynes JW: N epsilon-(carboxymethyl)lysine is a dominant advanced glycation end product (AGE) antigen in tissue proteins. *Biochemistry* 34:10872–10878, 1995
34. Schleicher ED, Wagner E, Nerlich AG: Increased accumulation of the glycoxidation product N(epsilon)- (carboxymethyl)lysine in human tissues in diabetes and aging. *J Clin Invest* 99:457–468, 1997
35. Like AA, Rossini AA: Streptozotocin-induced pancreatic insulitis: new model of diabetes mellitus. *Science* 193:415–417, 1976
36. Marden LJ, Quigley NC, Reddi AH, Hollinger JO: Temporal changes during bone regeneration in the calvarium induced by osteogenin. *Calcif Tissue Int* 53:262–268, 1993
37. Marden LJ, Hollinger JO, Chaudhari A, Turek T, Schaub RG, Ron E: Recombinant human bone morphogenetic protein-2 is superior to demineralized bone matrix in repairing craniotomy defects in rats. *J Biomed Mater Res* 28:1127–1138, 1994
38. Habeeb A: Determination of free amino groups in proteins by trinitrobenezenesilfonic acid. *Anal Biochem* 14:328–336, 1966
39. Ling X, Sakashita N, Takeya M, Nagai R, Horiuchi S, Takahashi K: Immunohistochemical distribution and subcellular localization of three distinct specific molecular structures of advanced glycation end products in human tissues. *Lab Invest* 78:1591–1606, 1998
40. Fehrenbach H, Kasper M, Tschernig T, Shearman MS, Schuh D, Muller M: Receptor for advanced glycation endproducts (RAGE) exhibits highly differential cellular and subcellular localisation in rat and human lung. *Cell Mol Biol (Noisy-le-grand)* 44:1147–1157, 1998
41. Bellows CG, Aubin JE, Heersche JN, Antosz ME: Mineralized bone nodules formed in vitro from enzymatically released rat calvaria cell populations. *Calcif Tissue Int* 38:143–154, 1986
42. Park L, Raman KG, Lee KJ, Lu Y, Ferran LJ, Jr, Chow WS, Stern D, Schmidt AM: Suppression of accelerated diabetic atherosclerosis by the soluble receptor for advanced glycation endproducts. *Nat Med* 4:1025–1031, 1998
43. Leiter EH, Prochazka M, Coleman DL: The non-obese diabetic (NOD) mouse. *Am J Pathol* 128:380–383, 1987
44. Katayama Y, Akatsu T, Yamamoto M, Kugai N, Nagata N: Role of nonenzymatic glycosylation of type I collagen in diabetic osteopenia. *J Bone Miner Res* 11:931–937, 1996
45. Katayama Y, Celic S, Nagata N, Martin TJ, Findlay DM: Nonenzymatic glycation of type I collagen modifies interaction with UMR 201–10B preosteoblastic cells. *Bone* 21:237–242, 1997
46. Takagi M, Kasayama S, Yamamoto T, Motomura T, Hashimoto K, Yamamoto H, Sato B, Okada S, Kishimoto T: Advanced glycation endproducts stimulate Interleukin-6 production by human bone derived cells. *J Bone Miner Res* 12:439–446, 1997
47. Neeper M, Schmidt AM, Brett J, Yan SD, Wang F, Pan YC, Elliston K, Stern D, Shaw A: Cloning and expression of a cell surface receptor for advanced glycosylation end products of proteins. *J Biol Chem* 267:14998–15004, 1992
48. Goodman WG, Hori MT: Diminished bone formation in experimental diabetes: relationship to osteoid maturation and mineralization. *Diabetes* 33:825–831, 1984
49. Wu K, Schubeck KE, Frost HM, Villanueva A: Haversian bone formation rates determined by a new method in a mastodon, and in human diabetes mellitus and osteoporosis. *Calcif Tissue Res* 6:204–219, 1970
50. McCarthy AD, Etcheverry SB, Cortizo AM: Advanced glycation endproduct-specific receptors in rat and mouse osteoblast-like cells: regulation with stages of differentiation. *Acta Diabetol* 36:45–52, 1999
51. Vlassara H, Fuh H, Makita Z, Krungkrai S, Cerami A, Bucala R: Exogenous advanced glycosylation end products induce complex vascular dysfunction in normal animals: a model for diabetic and aging complications. *Proc Natl Acad Sci U S A* 89:12043–12047, 1992
52. Vlassara H, Striker LJ, Teichberg S, Fuh H, Li YM, Steffes M: Advanced glycation end products induce glomerular sclerosis and albuminuria in normal rats. *Proc Natl Acad Sci U S A* 91:11704–11708, 1994
53. Yamamoto T, Ozono K, Miyauchi A, Kasayama S, Kojima Y, Shima M, Okada S: Role of advanced glycation end products in a dynamic bone disease in patients with diabetic nephropathy. *Am J Kidney Dis* 38: S161–S164, 2001